Yu-Shiba-Rusinov States in a Superconductor with Topological $\mathbb{Z}_2$ Bands

Ching-Kai Chiu[1,2] and Ziqiang Wang[3]
[1]*RIKEN Interdisciplinary Theoretical and Mathematical Sciences (iTHEMS), Wako, Saitama 351-0198, Japan*
[2]*Kavli Institute for Theoretical Sciences, University of Chinese Academy of Sciences, Beijing 100190, China*
[3]*Department of Physics, Boston College, Chestnut Hill, Massachusetts 02467, USA*

(Received 23 October 2021; revised 19 April 2022; accepted 26 April 2022; published 6 June 2022)

A Yu-Shiba-Rusinov (YSR) state is a localized in-gap state induced by a magnetic impurity in a superconductor. Recent experiments used an STM tip to manipulate the exchange coupling between an Fe adatom and the $FeTe_{0.55}Se_{0.45}$ superconductor possessing a $\mathbb{Z}_2$ nontrivial band structure with topological surface states. As the tip moves close to the single Fe adatom, the energy of the in-gap state modulates and exhibits a zero-energy crossing followed by an unusual return to zero energy, which cannot be understood by coupling the magnetic impurity to the superconducting topological surface Dirac cone. Here, we numerically and analytically study the YSR states in superconductors with nontrivial $\mathbb{Z}_2$ bands and show the emergence of the two zero-energy crossings as a function of the exchange coupling between the magnetic impurity and the *bulk* states. We analyze the role of the topological surface states and compare in-gap states to systems with trivial $\mathbb{Z}_2$ bands. The spin polarization of the YSR states is further studied for future experimental measurement.

DOI: 10.1103/PhysRevLett.128.237001

A magnetic impurity adatom deposited on a superconductor can induce an in-gap bound state, which is known as a Yu-Shiba-Rusinov (YSR) state [1–3]. It has been theoretically proposed that the arrangement of the YSR states on the superconductor surface can lead to topological superconductor platforms hosting Majorana zero modes [4–15]. The experimental progress serves as hints of the Majorana existence [16–19]. Understanding the fundamentals of the YSR state [20–22] is an important step toward understanding local excitations in superconductors and topological superconductivity.

Novel properties of the YSR states have been probed by a controlled approach of the STM tip to the magnetic FeP molecules adsorbed on the surface of conventional Pb(111) superconductors [23]. Modulating the tip distance by changing the conductance G of the tunnel barrier [Fig. 1(a)] can directly manipulate the exchange coupling of the magnetic FeP to the superconductor. Two consecutive zero-energy crossings were observed with increasing G [23]. Since the exchange of quasiparticle and quasihole occurs at zero energy, a zero-energy crossing corresponds to a first-order quantum phase transition. However, since the distance between the STM tip and FeP turned out to not be nonmonotonic [23], the two crossings may correspond to the same exchange coupling at a single transition. Recently, magnetic Fe adatoms deposited on the surface of Fe-based superconductor $FeTe_{0.55}Se_{0.45}$ were studied by STM using a similar technique [16]. A zero-energy crossing of the YSR states with increasing G was observed and accompanied by a monotonic decrease in the tip distance d to the magnetic Fe adatom. Surprisingly, further increasing the exchange coupling by reducing d causes the YSR states to reverse trajectories and return to zero energy, in striking contrast to the expected behavior in conventional superconductors [1–3]. The emergence of the zero-energy bound state as robust against further reduction of d was interpreted as evidence for the transition to the quantum anomalous vortex spontaneously nucleated at magnetic Fe impurities [4], trapping a vortex Majorana zero mode from the SC topological surface states [16]. What drives the return of the

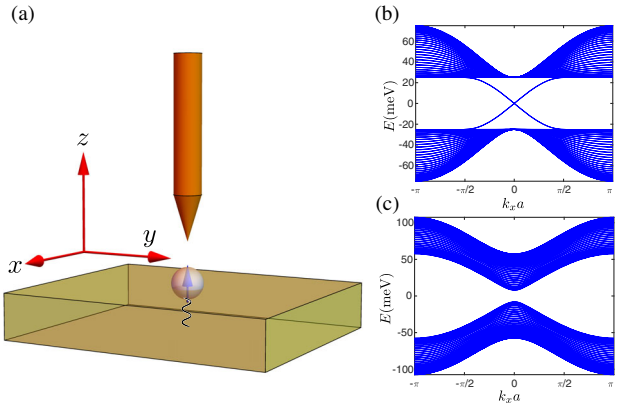

FIG. 1. (a) Schematic setup indicating an Fe adatom on the top surface of $FeTe_xSe_{1-x}$. The STM tip can be moved to approach the adatom, probing the tunneling current and manipulating the exchange coupling. (b) Bulk-surface spectrum at $k_y = 0$ for H_{TI}, showing the presence of the surface Dirac cone inside the $\mathbb{Z}_2$ nontrivial TI gap on the (001) surface at $m = 2$. (c) Spectrum of H_{TI} of the $\mathbb{Z}_2$ trivial insulator at $m = 3.3$, showing the bulk gap and the absence of the surface states.

YSR states to zero energy in a tendency to form a possible second zero-energy crossing was not understood.

In this Letter, we study the fundamental reason for the emergence of two zero-energy crossings of the YSR states as a function of exchange coupling in connection to $FeTe_{0.55}Se_{0.45}$. The nontrivial topological physics of $FeTe_{0.55}Se_{0.45}$ stems from the surface Dirac cone due to the topological $\mathbb{Z}_2$ bands, which becomes superconducting (SC) below the bulk T_c and can host Majorana zero modes in magnetic vortices [24–29]. In the effective surface-only theory, where the deposited magnetic impurity exchange couples to the SC Dirac cone exclusively, the in-gap YSR state exhibits only one zero-energy crossing [30], similar to the case of conventional superconductors [1–3]. The bulk physics and the possible emergence of another YSR state from the topological $\mathbb{Z}_2$ bands has not been studied.

We focus on the basic physics of the $\mathbb{Z}_2$ nontrivial band structure, by assuming the effects of the other bulk bands are small or at high energies. We thus consider a microscopic theory where the impurity spin is exchange coupled to the 3D $\mathbb{Z}_2$ bulk bands, and study the resulting localized in-gap states at the impurity. This procedure emphasizes that the interaction of the impurity spin with the topological surface states originates from its exchange coupling to the topological nontrivial bulk bands. Moreover, it captures the possible bulk physics that would be inaccessible in a surface-only effective model. We numerically and analytically study the entire 3D system modeled after $FeTe_{0.55}Se_{0.45}$ and reveal that the second zero-energy crossing comes from the bulk physics. We study and propose spin-polarized STM as a probe to distinguish the two zero-energy crossings.

We start with the Hamiltonian in momentum space describing a 3D strong topological insulator (TI) [31]

$$H_{\mathrm{TI}}(\boldsymbol{k}) = \nu_F M(\boldsymbol{k})\rho_z\sigma_0 - \mu\rho_0\sigma_0 + v_F \sin k_x a \rho_x\sigma_x + v_F \sin k_y a \rho_x\sigma_y + v_F \sin k_z a \rho_x\sigma_z, \quad (1)$$

where $M(\boldsymbol{k}) = -m + \cos k_x a + \cos k_y a - \cos k_z a$ and the Pauli matrices σ_α and ρ_β act in the spin and orbital space, respectively. Based on the experimental measurements [25,26], we choose the Fermi velocity $v_F = 25\ \mathrm{nm\,meV}/a$, wave vector $k_F = 0.2\ \mathrm{nm}^{-1}$, and the chemical potential $\mu = v_F/k_F = 5$ meV. For simplicity, we consider a simple cubic lattice and choose the lattice constant $a = 1$ nm in all directions (cf. [32]). Note that at $m = 3$, the bulk gap closes at Z point describing a bulk topological phase transition for $FeTe_{0.55}Se_{0.45}$. We therefore use $m = 2$ to describe the $\mathbb{Z}_2$ nontrivial bands where the surface Dirac cone emerges and maximally localizes on the surface, as shown in the bulk-surface spectrum in Fig. 1(b). The neutral point of the Dirac cone is located at $\bar{\Gamma}:(0,0)$ in the (001) surface BZ, which is consistent with $FeTe_xSe_{1-x}$. For comparison, we will also study the $\mathbb{Z}_2$ trivial bands at $m = 3.3$ shown in Fig. 1(c) where the gapless surface spectrum is absent. The superconducting topological surface states, as observed in $FeTe_{0.55}Se_{0.45}$, can be generated by introducing bulk s-wave superconductivity. The TI Hamiltonian is thus extended to the Bogoliubov-de Gennes (BdG) Hamiltonian

$$H^0_{\mathrm{BdG}} = \begin{pmatrix} H_{\mathrm{TI}}(\boldsymbol{k}) & -i\Delta_0\rho_0\sigma_y \\ i\Delta_0\rho_0\sigma_y & -H^*_{\mathrm{TI}}(-\boldsymbol{k}) \end{pmatrix}, \quad (2)$$

where the value of the SC gap, $\Delta_0 = 1.8$ meV, has been measured experimentally [25–27,33] and is used throughout the Letter.

We position the Fe adatom at the center of the (001) surface as shown in Fig. 1(a). An exchange coupling to the $\mathbb{Z}_2$ bands is induced at the center of the top surface, denoted as $\boldsymbol{r}_{\mathrm{top}} \equiv \boldsymbol{0}$. Since the lattice translation symmetry is broken, it is necessary to rewrite the BdG Hamiltonian in the real space

$$\hat{H}_{\mathrm{BdG}} = \sum_{\boldsymbol{r}} \begin{pmatrix} c^\dagger_{\boldsymbol{r}} & c_{\boldsymbol{r}} \end{pmatrix} \begin{pmatrix} H_0(m) & -i\Delta_0\rho_0\sigma_y \\ i\Delta_0\rho_0\sigma_y & -H^*_0(m) \end{pmatrix} \begin{pmatrix} c_{\boldsymbol{r}} \\ c^\dagger_{\boldsymbol{r}} \end{pmatrix} + \sum_{\boldsymbol{r},\boldsymbol{\delta}} \begin{pmatrix} c^\dagger_{\boldsymbol{r}} & c_{\boldsymbol{r}} \end{pmatrix} \begin{pmatrix} H_{\mathrm{nn}}(\boldsymbol{\delta}) & 0 \\ 0 & -H^*_{\mathrm{nn}}(\boldsymbol{\delta}) \end{pmatrix} \begin{pmatrix} c_{\boldsymbol{r}+\boldsymbol{\delta}} \\ c^\dagger_{\boldsymbol{r}+\boldsymbol{\delta}} \end{pmatrix}, \quad (3)$$

where the on-site part $H_0(m) = v_F m\rho_z\sigma_0 - \mu\rho_o\sigma_0 + M_z\rho_0\sigma_z\delta(\boldsymbol{r} - \boldsymbol{r}_{\mathrm{top}})$ contains the spin exchange coupling M_z taken to be along the z direction first. Here we assume each orbital has the same strength exchange coupling and the Supplemental Material [34] shows the simulation for different orbital strengths. In the nearest neighbor hopping part, $\boldsymbol{\delta} = \pm a\hat{x}, \pm a\hat{y}, \pm a\hat{z}$ indicates the three directions of the hopping, and $H_{\mathrm{nn}}(\pm a\hat{n}) = -v_F\rho_z\sigma_0/2 \pm iv_F\rho_x\sigma_n/2$ for $n = x, y, z$.

Since the YSR state is localized on the top surface, the surface size ($L_xL_ya^2$) and the number of layers L_z in the z direction do not significantly affect this in-gap bound state. Hence, we choose $L_x = L_y = 80$ and $L_z = 5$ for the following simulations. By performing the Lanczos algorithm, we find states $\Psi_j(\boldsymbol{r}) = [\boldsymbol{u}_j(\boldsymbol{r}), \boldsymbol{v}_j(\boldsymbol{r})]$ within and near the SC gap. Figure 2(a) shows the evolution of the lowest energy eigenstates as the exchange coupling M_z increases from 0. The trajectories within the superconductor gap (1.8 meV) correspond to those of the YSR states localized near the Fe adatom, which indeed exhibit two zero-energy crossings. Figure 2(b) shows the LDOS at the adatom ($\boldsymbol{r} = \boldsymbol{0}$) given by

$$N(\boldsymbol{r}, E) = \sum_{E_j<0} \left[\frac{|\boldsymbol{u}_j(\boldsymbol{r})|^2}{\cosh^2[\beta(E - E_j)]} + \frac{|\boldsymbol{v}_j(\boldsymbol{r})|^2}{\cosh^2[\beta(E + E_j)]} \right]$$

and $1/\beta = k_BT = 0.05$ meV. The spin-resolved LDOS $(N_\uparrow, N_\downarrow)$ can be computed by selecting the designated

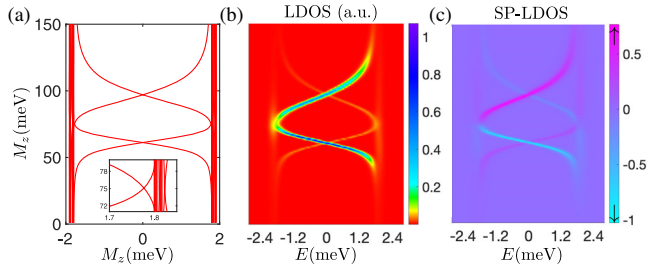

FIG. 2. Evolution of the YSR states with increasing exchange coupling ($\mu = 5$ meV, $m = 2$, and $M_x = M_y = 0$). (a) Spectrum of the in-gap states, showing that YSR states pass through zero-energy twice. The inset shows that the crossing near the gap edge is formed by the first YSR state moving up and a new YSR state moving down in energy. (b) At nonzero exchange couplings, the intensity of the YRS state in the LDOS N breaks particle-hole symmetry. The coherence peaks associated with the SC gap cannot be seen clearly due to the dominating spectral weight of the YSR states. (c) The normalized spin-resolved LDOS N_p. The highest peak is spin-down polarized at small to moderate M_z, and another main YSR peak with spin-up polarization moves from $-\Delta_0$ to Δ_0.

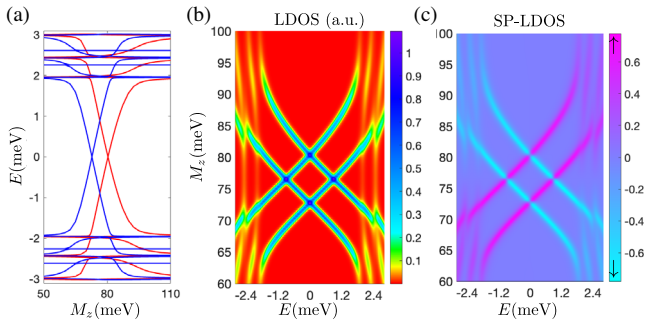

FIG. 3. Evolution of the YSR states at zero chemical potential ($\mu = 0$, $m = 2$, and $M_x = M_y = 0$). (a) Spectra of the two decoupled Hamiltonian blocks are separately represented by blue lines (H_+) and red lines (H_-). Each block contributes one zero-energy crossing for $M_z > 0$. (b) LDOS shows the spectral weight of the YSR states are perfectly particle-hole symmetric. (c) SP-LDOS shares similar features to the case at $\mu = 5$ meV.

spin part. The normalized spin-polarized (SP) LDOS $N_p = (N_\uparrow - N_\downarrow)/\sqrt{N_\uparrow + N_\downarrow}$ is plotted in Fig. 2(c) at $\boldsymbol{r} = \boldsymbol{0}$. Starting from the weak exchange coupling M_z, the LDOS of the YSR states exhibits particle-hole symmetric peak energy positions but with asymmetric spectral intensity [Fig. 2(b)]. Figure 2(c) shows that the highest peak, which is spin-down polarized at positive energy, is much higher than the spin-up polarized second highest peak at negative energy. As M_z increases, these two peaks move close to each other and then cross the Fermi level at zero energy. As the main peak continues to move toward $-\Delta_0$, the second peak moves toward Δ_0.

Surprisingly, contrary to the expected behavior where the two peaks merge into the continuum at $\pm\Delta_0$ with further increasing of the exchange coupling, another YSR state emerges from the continuum and the two distinct YSR states form an energy crossing just inside the SC gap as shown in the inset in Fig. 2(a). Moreover, the newly emerged YSR state in Fig. 2(c) an opposite spin polarization such that the main peak becomes spin-up polarized and moves from $-\Delta_0$ to Δ_0 with increased M_z as can be seen in Fig. 2(b), while the spin-down polarized second peak moves in the opposite direction. This creates a remarkable second zero-energy crossing in the trajectories of the YSR states displayed in Fig. 2. The Supplemental Material [34] shows the spatial line cuts at the two crossings. Figure 2 shows that the crossings are located at $M_z^{c1} = 61$ meV and $M_z^{c2} = 97$ meV, which are close to the estimated exchange coupling from the neutron scattering experiments ($\sim$70 meV [35]).

The presence of two zero-energy crossings hints at the new physics of the YSR states in superconductors with topological $\mathbb{Z}_2$ bands that is beyond the description by only the SC surface Dirac cone [30]. To understand the physical origin of the two zero-energy crossings, we include the in-plane exchange couplings (M_x, M_y) and rewrite the real-space BdG Hamiltonian (3) in momentum space by introducing the Pauli matrices τ_α acting in the particle-hole sector,

$$\begin{aligned} H_{\mathrm{BdG}} = {} & v_F M \tau_z \rho_0 \sigma_0 + v_F \sin k_x \tau_0 \rho_x \sigma_x + v_F \sin k_y \tau_z \rho_x \sigma_y \\ & + v_F \sin k_z \tau_0 \rho_x \sigma_z + \Delta_0 \tau_y \rho_0 \sigma_y \\ & + \delta(\boldsymbol{r})(M_x \tau_z \rho_0 \sigma_x + M_y \tau_0 \rho_0 \sigma_y + M_z \tau_z \rho_0 \sigma_z), \end{aligned} \quad (4)$$

where the chemical potential μ has been set to zero for simplicity. Note that H_{BdG} has an emergent symmetry and commutes with the operator $P = \tau_y \rho_y \sigma_y$. As a result, the Hamiltonian can be block diagonalized under the unitary transformation $\bar{H}_{\mathrm{BdG}} = \mathrm{diag}(H_+, H_-)$ [34], where

$$\begin{aligned} H_\pm(\boldsymbol{k}) = {} & \mp v_F M \rho_y \sigma_y + v_F \sin k_x \rho_0 \sigma_x - v_F \sin k_y \rho_z \sigma_y \\ & \mp v_F \sin k_z \rho_x \sigma_y \pm \Delta_0 \rho_0 \sigma_z \\ & + \delta(\boldsymbol{r})(\pm M_x \rho_y \sigma_0 \pm M_y \rho_x \sigma_z - M_z \rho_z \sigma_z). \end{aligned} \quad (5)$$

First, we only consider the out-of-plane exchange coupling ($M_x = M_y = 0$). The numerical result in Fig. 3 shows that the YSR states still exhibit two zero-energy crossings as a function of M_z in this case. Intriguingly, Fig. 3(a) reveals that the two crossings respectively stem from the two different Hamiltonian blocks $H_\pm$. Furthermore, while the spin polarizations of the YSR states in Fig. 3(c) are similar to those at $\mu = 5$ meV displayed in Fig. 2(b), the spectral weights of the LDOS peaks are different and appear perfectly particle-hole symmetric as shown in Fig. 3(b). This additional symmetry originates from the fact that P

connects particle and hole wave functions and in the eigenbasis of P, $|\boldsymbol{u}^{\uparrow}|^2+|\boldsymbol{u}^{\downarrow}|^2=|\boldsymbol{v}^{\uparrow}|^2+|\boldsymbol{v}^{\downarrow}|^2$.

The block-diagonal Hamiltonian H_+ and H_- can be identified as partners of an effective time reversal symmetry T. This amounts to

$$\rho_z\sigma_y H_+^*(-\boldsymbol{k},-M_z)\rho_z\sigma_y=H_-(\boldsymbol{k},M_z) \tag{6}$$

such that the YSR state generated by M_z in H_+ can be easily transformed to the one generated by $-M_z$ in H_-. In the Supplemental Material [34], we take the continuum limit of $H_\pm$ and provide an approximate, but rather general, analytical solution of the critical exchange couplings for the zero-energy crossings. For our topological $\mathbb{Z}_2$ bands at $m=2$, the zero-energy YSR states appear for $H_\pm$ at

$$M_{z,\alpha}^{\pm}=\pm\frac{(-1)^{\alpha-1}4\pi v_F^2}{\Delta_0\ln[1+\frac{\Lambda^2 v_F^2}{\Delta_0^2+(1-\alpha)v_F^2}]},\qquad \alpha=1,2, \tag{7}$$

where Λ is the momentum cutoff. The order of the exchange couplings corresponding to the zero-energy crossings is given by $M_{z,2}^{+}<M_{z,1}^{-}<0<M_{z,1}^{+}<M_{z,2}^{-}$. This analytic solution shows that there are two zero-energy crossings for each impurity polarization direction, i.e., each sign of M_z, and for $M_z>0$ the first (second) crossing belongs to H_+ (H_-), which are consistent with the simulation results shown in Fig. 3.

Since the YSR states are localized at the Fe adatom on the top surface, additional insights can be gained from the analytical solution. At $m=2$ and on the top surface, the first 2×2 blocks of H_+ and H_-, which are separately isolated, represent the physics of the SC surface Dirac cone and lead to the zero-energy YSR state at $M_{z,1}^{+}>0$ and $M_{z,1}^{-}<0$ [34]. This part corresponds to what is captured in an effective theory with the SC topological surface Dirac cone alone [30]. The second zero-energy crossing at $M_{z,2}^{-}>0$ and $M_{z,2}^{+}<0$ emerges from the remaining block of the Hamiltonian and involves the coupling of the magnetic impurity to the bulk bands at the surface. This is ultimately related to the strongly spin-orbit coupled two-orbitals of the nontrivial $\mathbb{Z}_2$ band structure with band inversion. We have verified that the two zero-energy crossings of the YSR states as a function of the exchange coupling remain robust when the Fermi level crosses the bulk band [34]. For completeness, we have studied the model at $m=3.3$ [Fig. 1(c)], where the $\mathbb{Z}_2$ bands are topologically trivial with the absence of band inversion and Dirac cone surface states, and found very different behaviors both numerically and analytically [34]. Unlike YSR states with a particle or hole counterpart, as the chemical potential is adjusted within the bulk gap in the trivial platform, the in-gap states are localized magnetic states without a particle or hole counterpart. These states still exhibit the two artificial zero-energy crossings in the BdG Hamiltonian and the $\mathbb{Z}_2$ index only affects the physical form of the in-gap states.

To show that the origin of the two zero-energy crossings stems from the two orbitals, let's consider the limit where the exchange coupling M_z from a single magnetic impurity goes to $+\infty$. In this limit, the total angular momentum (J_z) in the z direction must be reduced by $2\times\hbar/2$ due to the spin flip in the two orbitals, compared to the system without the magnetic impurity. As discussed in the Supplemental Material [34], each zero-energy crossing leads to a $-\hbar/2$ change in the angular momentum. Thus, there must be two zero-energy crossings.

We have studied the physics of the YSR states induced by a magnetic impurity in s-wave superconductors with topological nontrivial $\mathbb{Z}_2$ bands. Our findings of two YSR states that evolve with exchange coupling and exhibit two zero-energy crossings are consistent with the experimental observations at the Fe adatoms deposited on the surface of $FeTe_{0.55}Se_{0.45}$ superconductors [16]. A closer comparison reveals that after the first zero-energy crossing, in the experiment [16] the energy of the YSR state remains in the SC gap away from the continuum, which deviates from the behavior shown in Fig. 2(a), where the inset displays the two YSR states crossing each other without hybridization at the gap edge. We argue that the absence of the YSR crossing is due to the canting of the magnetic moment of the Fe adatom away from the z direction, which induces an important in-plane component of the exchange coupling (M_x, M_y). In Fig. 4, we show the evolution of the YSR states induced by the exchange coupling $M_x\tau_z\rho_0\sigma_x$ along the x direction, while other parameters are the same as in Fig. 2. Figures 4(a) and 4(b) show that after the first crossing, the energy of the YSR state stays inside the SC gap and forms the second crossing, as the exchange coupling increases. Thus, the exchange coupling in the

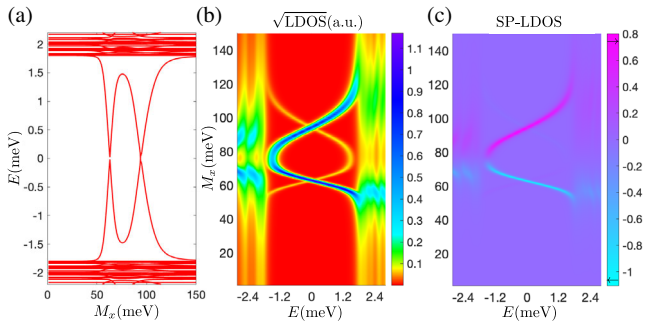

FIG. 4. Evolution of the YSR states with *in-plane* exchange coupling M_x ($\mu=5$ meV, $m=2$, and $M_y=M_z=0$). (a) Between the two zero-energy crossings, the YSR states evolve inside the SC gap with increasing M_x. (b) LDOS at the magnetic impurity showing the spectral weight of the YSR states. A square root scale bar is used to reveal the small particle-hole counterpart of the peak. (c) SP-LDOS showing the YSR state changes from spin-left ($-x$) to spin-right ($+x$) polarization after bending back.

in-plane direction brings consistency with the experiments. The reason is that the in-plane exchange coupling M_x and finite chemical potential $\mu \neq 0$ [34] lead to the hybridization of the two YSR states so that the crossing point at the finite energy in the inset in Fig. 2(a) is gapped and the new YRS state bends back to form the second zero-energy crossing. The agreement further supports the experimental observed evolution of the in-gap states as the novel YSR states in a superconductor with a topological nontrivial $\mathbb{Z}_2$ band structure.

We considered only the already challenging vortex-free solution and found that the YSR bound states generically exhibit two zero-energy crossings with increasing exchange coupling. The predicted second crossing at a larger exchange coupling is not seen experimentally [16], but replaced instead by the coalescing of YSR states at zero energy and the pinning of the zero-energy bound states with further increasing of the exchange coupling. This discrepancy indicates that increasing the normal state conductance, the experiments observed a transition out of the vortex-free YSR states, and mostly likely into a quantum anomalous vortex state [4] hosting a Majorana zero mode.

Our findings also shed light on the experimental detection of the YSR states using spin-polarized STM. In the experiment using spin-polarized STM, but without pushing the tip closer to the Fe adatoms [36], the exchange coupling of the Fe magnetic moment may not be strong enough to cause the YSR state to pass through the first crossing. Therefore, the highest peak of the LDOS inside the SC gap has spin-down polarization and appears at a positive energy, while the second-highest peak with spin-up polarization is located at the opposite negative energy. In reality, the STM tip is not 100% polarized (the polarization is presumably less 10%). Even if the LDOS peaks are 100% polarized, the spin-polarized STM tip may pick up only a small difference between the two spins directions, which may be responsible for the current experimental observation. Our findings suggest that the spin-polarized STM tip can be used to distinguish the two energy crossings as the tip distance is reduced. As shown in Fig. 2(c), the main peak near the first crossing is spin-down polarized, while it becomes spin-up polarized near the second crossing. A spin check in the future can confirm the monotonically increasing exchange coupling with the decreasing tip distance [16]. Finally, the recent ultrahigh-resolution STM experiments show multiple YSR states inside the SC gap of $FeTe_{0.55}Se_{0.45}$ [37]. Our results hint at the emergence of multiple YSR states from additional bulk bands derived from other atomic orbitals.

We would like to thank Tadashi Machida, Kun Jiang, Shuheng Pan, and Dongfei Wang for insightful discussions. Z. W. acknowledges the support of the U.S. DOE, Basic Energy Sciences Grant No. DE-FG02-99ER45747.

[1] L. Yu, Acta Phys. Sin **21**, 75 (1965), https://www.osti.gov/biblio/4638963.
[2] H. Shiba, Prog. Theor. Phys. **40**, 435 (1968).
[3] A. I. Rusinov and P. M. Z. E. T. Fiz, JETP Lett. **9** (1968), http://jetpletters.ru/ps/1658/article 25295.shtml.
[4] K. Jiang, X. Dai, and Z. Wang, Phys. Rev. X **9**, 011033 (2019).
[5] M. Schecter, K. Flensberg, M. H. Christensen, B. M. Andersen, and J. Paaske, Phys. Rev. B **93**, 140503(R) (2016).
[6] M. M. Vazifeh and M. Franz, Phys. Rev. Lett. **111**, 206802 (2013).
[7] I. Reis, D. J. J. Marchand, and M. Franz, Phys. Rev. B **90**, 085124 (2014).
[8] S. Nakosai, Y. Tanaka, and N. Nagaosa, Phys. Rev. B **88**, 180503(R) (2013).
[9] C.-K. Chiu, G. Bian, H. Zheng, J.-X. Yin, S. S. Zhang, D. S. Sanchez, I. Belopolski, S.-Y. Xu, and M. Z. Hasan, Europhys. Lett. **123**, 47005 (2018).
[10] J. Li, T. Neupert, Z. Wang, A. H. MacDonald, A. Yazdani, and B. A. Bernevig, Nat. Commun. **7**, 12297 (2016).
[11] F. Pientka, L. I. Glazman, and F. von Oppen, Phys. Rev. B **88**, 155420 (2013).
[12] J. Klinovaja, P. Stano, A. Yazdani, and D. Loss, Phys. Rev. Lett. **111**, 186805 (2013).
[13] R. Pawlak, M. Kisiel, J. Klinovaja, T. Meier, S. Kawai, T. Glatzel, D. Loss, and E. Meyer, npj Quantum Inf. **2**, 16035 (2016).
[14] L. A. Wray, S.-Y. Xu, Y. Xia, Y. S. Hor, D. Qian, A. V. Fedorov, H. Lin, A. Bansil, R. J. Cava, and M. Z. Hasan, Nat. Phys. **6**, 855 (2010).
[15] S. Sasaki, M. Kriener, K. Segawa, K. Yada, Y. Tanaka, M. Sato, and Y. Ando, Phys. Rev. Lett. **107**, 217001 (2011).
[16] P. Fan, F. Yang, G. Qian, H. Chen, Y.-Y. Zhang, G. Li, Z. Huang, Y. Xing, L. Kong, W. Liu, K. Jiang, C. Shen, S. Du, J. Schneeloch, R. Zhong, G. Gu, Z. Wang, H. Ding, and H.-J. Gao, Nat. Commun. **12**, 1348 (2021).
[17] H. Kim, A. Palacio-Morales, T. Posske, L. Rózsa, K. Palotás, L. Szunyogh, M. Thorwart, and R. Wiesendanger, Sci. Adv. **4**, eaar5251 (2018).
[18] A. Palacio-Morales, E. Mascot, S. Cocklin, H. Kim, S. Rachel, D. K. Morr, and R. Wiesendanger, Sci. Adv. **5**, eaav6600 (2019).
[19] S. Nadj-Perge, I. K. Drozdov, J. Li, H. Chen, S. Jeon, J. Seo, A. H. MacDonald, B. A. Bernevig, and A. Yazdani, Science **346**, 602 (2014).
[20] T. Meng, J. Klinovaja, S. Hoffman, P. Simon, and D. Loss, Phys. Rev. B **92**, 064503 (2015).
[21] H. Kim, L. Rózsa, D. Schreyer, E. Simon, and R. Wiesendanger, Nat. Commun. **11**, 4573 (2020).
[22] P. Beck, L. Schneider, L. Rózsa, K. Palotás, A. Lászlóffy, L. Szunyogh, J. Wiebe, and R. Wiesendanger, Nat. Commun. **12**, 2040 (2021).
[23] L. Farinacci, G. Ahmadi, G. Reecht, M. Ruby, N. Bogdanoff, O. Peters, B. W. Heinrich, F. von Oppen, and K. J. Franke, Phys. Rev. Lett. **121**, 196803 (2018).
[24] L. Fu and C. L. Kane, Phys. Rev. Lett. **100**, 096407 (2008).

[25] P. Zhang, K. Yaji, T. Hashimoto, Y. Ota, T. Kondo, K. Okazaki, Z. Wang, J. Wen, G. D. Gu, H. Ding, and S. Shin, Science **360**, 182 (2018).
[26] D. Wang, L. Kong, P. Fan, H. Chen, S. Zhu, W. Liu, L. Cao, Y. Sun, S. Du, J. Schneeloch, R. Zhong, G. Gu, L. Fu, H. Ding, and H.-J. Gao, Science **362**, 333 (2018).
[27] T. Machida, Y. Sun, S. Pyon, S. Takeda, Y. Kohsaka, T. Hanaguri, T. Sasagawa, and T. Tamegai, Nat. Mater. **18**, 811 (2019).
[28] C.-K. Chiu, T. Machida, Y. Huang, T. Hanaguri, and F.-C. Zhang, Sci. Adv. **6**, eaay0443 (2020).
[29] L. Kong, L. Cao, S. Zhu, M. Papaj, G. Dai, G. Li, P. Fan, W. Liu, F. Yang, X. Wang, S. Du, C. Jin, L. Fu, H.-J. Gao, and H. Ding, Nat. Commun. **12**, 4146 (2021).
[30] A. A. Zyuzin and D. Loss, Phys. Rev. B **90**, 125443 (2014).
[31] H. Zhang, C.-X. Liu, X.-L. Qi, X. Dai, Z. Fang, and S.-C. Zhang, Nat. Phys. **5**, 438 (2009).
[32] S. Li, C. de la Cruz, Q. Huang, Y. Chen, J. W. Lynn, J. Hu, Y.-L. Huang, F.-C. Hsu, K.-W. Yeh, M.-K. Wu, and P. Dai, Phys. Rev. B **79**, 054503 (2009).
[33] M. Chen, X. Chen, H. Yang, Z. Du, X. Zhu, E. Wang, and H.-H. Wen, Nat. Commun. **9**, 970 (2018).
[34] See Supplemental Material at http://link.aps.org/supplemental/10.1103/PhysRevLett.128.237001 for (1) additional properties of YSR states at zero-energy crossings, (2) the analytic derivation for the two zero-energy crossings stemming from the surface and bulk bands, (3) the YSR state evolution with the Fermi level crossing the bulk bands, (4) the YSR states in the $\mathbb{Z}_2$ trivial region, (5) the absence of the energy crossing at finite energy between the two zero-energy crossings.
[35] V. Thampy, J. Kang, J. A. Rodriguez-Rivera, W. Bao, A. T. Savici, J. Hu, T. J. Liu, B. Qian, D. Fobes, Z. Q. Mao, C. B. Fu, W. C. Chen, Q. Ye, R. W. Erwin, T. R. Gentile, Z. Tesanovic, and C. Broholm, Phys. Rev. Lett. **108**, 107002 (2012).
[36] D. Wang, J. Wiebe, R. Zhong, G. Gu, and R. Wiesendanger, Phys. Rev. Lett. **126**, 076802 (2021).
[37] Tadashi Machida (private communication).